ＩＳＳＮ１３４６－７８３２

独立行政法人港湾空港技術研究所

港湾空港技術研究所報告

REPORT OF
THE PORT AND AIRPORT RESEARCH
INSTITUTE

VOL.50　No.1　March　2011

NAGASE,YOKOSUKA,JAPAN

INDEPENDENT ADMINISTRATIVE INSTITUTION,
PORT AND AIRPORT RESEARCH INSTITUTE

港湾空港技術研究所報告（REPORT OF PARI）

第 50 巻　第 1 号（Vol. 50,　No. 1），　2011 年3月（March 2011）

目　　次（CONTENTS）

REPORT OF THE PORT AND
AIRPORT RESEARCH INSTITUTE
Vol. 50, No.1 (Mar .2011)

Effect of Surface Improvement Layer on Internal Stability of Group Column Type Deep Mixing Improved Ground under Embankment Loading

Masaki KITAZUME*

Synopsis

The Deep Mixing Method (DMM), an in situ soil stabilization technique using cement and/or lime as a binder, is often applied to improve soft soils. The group column type pattern is extensively applied to stabilize the foundation for embankments or lightweight structures. An improved ground design procedure, established in Japan, assumes two failure patterns related to external and internal stability. The author previously conducted a research project on the failure mechanism and stability of group column type improved ground subjected to embankment loading. The project involved the investigation of failure pattern and criteria for the two stability analyses, and the research results have been presented: the DM columns exhibited an overturning failure pattern in the case of high column strength and a bending failure pattern in the case of low column strength.

In the present study, a series of model tests was conducted to investigate the effect of a surface improvement layer on embankment stability, where the surface improvement layer was constructed to connect the DM columns. The test results shows that the surface layer has the effect to increase the embankment pressure at ground failure about 15 to 35% than that without the surface improvement layer. A simple calculation based on the bending failure mode of the columns was proposed and revealed high applicability for evaluating the internal stability of the improved ground. This paper describes the failure modes of the DM columns and a proposed simple calculation that incorporates the effect of the surface improvement layer.

Key Words: centrifuge model test, deep mixing soil stabilization, surface improvement layer, embankment, failure, soft ground, stability

* Distinguished Researcher, Port and Airport Research Institute, 3-1-1 Nagase, Yokosuka 239-0826, Japan
Phone: +81-46-844-5089 Fax: +81-46-844-0255 E-mail: kitazume@pari.go.jp

港湾空港技術研究所報告
第 50 巻第 1 号(2011.3)

盛土荷重を受ける杭式深層混合処理地盤の内部安定への表層処理層の効果

北詰　昌樹*

要　旨

深層混合処理工法（DMM）は，これまで軟弱地盤の改良に広く適用されてきている．深層混合処理工法による改良パターンの中で，杭式改良地盤は盛土や比較的軽量の構造物の基礎地盤の改良などに用いられている．杭式改良地盤に関する現行設計法では，外部安定および内部安定の検討を行っている．これまで，筆者は，盛土荷重下の杭式改良地盤の外部安定性と内部安定性に着目し，改良地盤の改良幅，改良率および改良杭の強度を変化させた遠心模型実験を行うとともに，簡単な安定計算を提案してきた．

本研究では，盛土荷重下の杭式改良地盤の安定性に及ぼす表層処理層の効果について遠心模型実験で検討した．実験から，表層処理層を有する改良地盤は，表層処理層のない場合に比べ，破壊盛土圧力が 15～35%程度大きいことが分かった．実験で得られた改良地盤の破壊パターンを基に簡単な安定計算法を提案し，その妥当性を示すとともに改良地盤の破壊メカニズムについて検討した．本論文では，遠心模型実験の準備ならびに実験結果，提案した安定計算法の基本的な考え方などを記述した．

キーワード：深層混合処理工法，盛土，安定性，破壊，遠心模型実験，数値解析

*　研究主監
〒239-0826　横須賀市長瀬3-1-1　独立行政法人港湾空港技術研究所
電話：046-844-5089　Fax：046-844-0255　　e-mail:kitazume@pari.go.jp

Contents

1. INTRODUCTION

The Deep Mixing Method (DMM), an in situ soil stabilization technique using cement and/or lime as a binder, is often applied to improve soft soils (Coastal Development Institute of Technology, 2002). The group column type pattern is extensively applied to stabilize the foundation for embankments or lightweight structures. An improved ground design procedure, established in Japan mainly for reinforcing embankments (Public Works Research Center, 2004), assumes two failure patterns related to external and internal stability. External stability is evaluated for potential sliding failure, in which the DM columns and the clay between the columns show horizontal displacement on a stiff layer without any rearrangement of columns. For internal stability, the potential for rupture breaking failure is evaluated by slip circle analysis, assuming the shear failure mode of DM columns (Fig. 1).

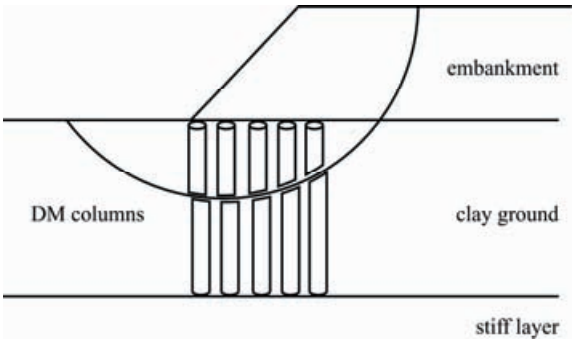

Fig. 1. Assumed failure pattern of DM improved ground for internal stability in the current design method.

Kitazume et al. (1991, 2000) performed a series of centrifuge model tests to assess the external stability of a breakwater on column-type DM ground reaching a stiff layer, and demonstrated that collapse failure, where the columns tilt like dominos at the bottom, could take place instead of sliding failure. Kitazume and Maruyama (2005, 2006) performed another series of centrifuge model tests and proposed a design method for external stability by incorporating the collapse failure pattern.

For internal stability, Terashi and Tanaka (1983), Miyake et al. (1991), Karastanev et al. (1997), Hashizume et al. (1998) and Kitazume et al. (1996, 1999) carried out model tests in which the DM columns exhibited various failure modes: shear, bending and tensile failure, depending not only on the ground and loading conditions but also on the location of each column. However, the current design method incorporates only the effect of the shear failure mode. As the bending and tensile strength of stabilized soil is much lower than the compressive strength (Terashi et al., 1980), the current design method based on the shear strength alone might overestimate the internal stability. Kivelo (1998) and Broms (2004) proposed a new design method for group column type improved ground, in which several failure modes of DM columns are taken into account.

The author previously conducted a research project on the failure mechanism and stability of group column type improved ground subjected to embankment loading. The project involved the investigation of failure pattern and criteria for the two stability analyses. The research results on the external and internal stability have been presented (Kitazume and Maruyama, 2006, 2007; Kitazume, 2008). These investigations revealed that the DM columns exhibit an overturning failure pattern in the case of high column strength and a bending failure pattern in the case of low column strength. Furthermore, the group columns that exhibited overturning or bending failure did not show a significant increase in stability even with an increase in column strength, while the columns that exhibited sliding or shear failure showed a large increase in stability. The surface improvement layer was expected to change the failure mode and in turn increase the stability.

In the present study, a series of model tests was conducted to investigate the effect of a surface improvement layer on embankment stability, where the surface improvement layer was designed to connect the DM columns. This paper describes the failure mode of the DM columns and a proposed simple calculation that incorporates the effect of the surface improvement layer.

2. CENTRIFUGE MODEL TESTS

2.1 Apparatus and model ground preparation

A series of model tests was carried out in the Mark II geotechnical centrifuge at the Port and Airport Research Institute (Kitazume and Miyajima, 1995). A specimen strong box with inside dimensions of 70 cm in length, 20 cm in width and 60 cm in depth was used for all model tests. Figure 2 shows a typical example of the model ground setup, in which normally consolidated clay ground 20 cm thick, five rows of DM columns and a surface improvement layer are modeled. Details of the model ground preparation for Cases 1 to 11 have been explained in previous reports (Kitazume and Maruyama, 2006, 2007) and the model ground preparation for Case 12, with the surface improvement layer, is briefly described below.

After the self-weight consolidation of a clay layer, the centrifuge was stopped once for the preparation of improved ground on the laboratory floor. A thin-walled tube with an outer diameter of 20 mm was inserted into the clay ground. The clay in the tube was then carefully removed using a tiny auger to make holes, and a model DM column was inserted after removing the tube. This procedure was repeated to produce improved ground in a square pattern with an interval of 33 mm, as shown in the upper part of Fig. 2. The improvement area ratio, a_s, was defined as the ratio of the sectional area of DM column to the hypotheti-

cal cylindrical area (CDIT, 2002), and was 0.28 in this study. The cement-stabilized column, Tl, was used for investigating the internal stability by simulating rupture breaking failure of DM columns, as shown in Table 1.

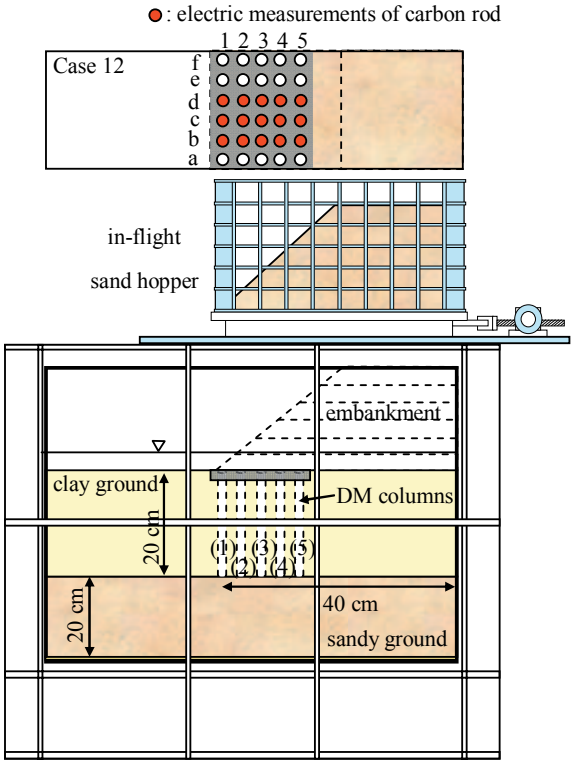

Fig. 2. Model ground setup for Case 12.

After inserting DM columns in the holes, the clay surface was locally excavated to a width of 16.5 cm and depth of 2 cm and the cement-stabilized mixture was poured into it. The mixing conditions for the DM columns and surface improvement layer are summarized in Table 1.

Several earth pressure gauges were placed at the top of the surface improvement layer at the model column and the clay between in order to investigate the stress concentration phenomenon during embankment loading. The embankment was constructed on the model ground by means of an in-flight sand-raining device in a 50-*g* acceleration field.

Table 1. Engineering properties of model columns.

Name	Material	Carbon rod		Model column			
				Mixing conditions		Strength	
		Diam.	Strength	w_i	aw	q_u	σ_b
		(mm)	(MN/m^2)	(%)	(%)	(kN/m^2)	(kN/m^2)
A	Acrylic	-	-	-	-	-	-
Tl	Stabilized soil	2	62.6	160	12.5	409	132
Th	Stabilized soil	3.2	34.5	160	10.0	1332	331

3. TEST RESULTS

3.1 Embankment pressure and displacement

The embankment pressure, p_e, and horizontal displacement, δ_h, curve in Case 12 is shown in Fig. 3, together

Table 2. Test conditions and major test results.

	Improvement conditions							Test results
	Width	Number of rows	Improve. area ratio, a_s	Material	DM column		Surface layer	Embk. pressure at failure, p_{ef}
					q_u	σ_b	q_u	
	(cm)				(kN/m^2)	(kN/m^2)	(kN/m^2)	(kN/m^2)
Case 1	0	-	-	-	-	-	-	10.8*
Case 2	8.6	3	0.28	A	-	-	-	26.5*
Case 3	15.2	5	0.28	A	-	-	-	42.2*
Case 4	21.8	7	0.28	A	-	-	-	50.0*
Case 6	8.6	3	0.28	Tl	425	122	-	16.9–23.7
Case 7	15.2	5	0.28	Tl	411	131	-	26.2–35.3
Case 8	21.8	7	0.28	Tl	391	142	-	25.4–32.6
Case 9	8.6	3	0.28	Th	1271	312	-	33.3–49.7
Case 10	15.2	5	0.28	Th	1290	367	-	34.2–50.2
Case 11	21.8	7	0.28	Th	1434	316	-	47.9–68.5
Case 12	15.2	5	0.28	Tl	420	133	289	30.3–47.6

with the unimproved ground (Case 1) and the improved ground without a surface improvement layer (Case 7). In the figure, the vertical axis shows the embankment pressure measured at the ground surface, p_e, and the horizontal axis shows the horizontal displacement at the toe of the embankment slope, δ_h.

In the unimproved ground (Case 1), a relatively small horizontal displacement took place as long as p_e remained at a very low level, but δ_h increased rapidly with further increase in p_e. In the improved ground without the surface improvement layer (Case 7), δ_h increased with increasing p_e, and its magnitude was almost of the same order as that of the unimproved ground as far as it was tested. In Case 12, with the surface improvement layer, δ_h increased gradually with increasing p_e, and its magnitude was smaller than that in the above two cases. Comparing the magnitude of horizontal displacement at p_e of about 45 kN/m^2, when the embankment loading in Case 7 was terminated, δ_h in Case 12 was about 50% of that in Case 7 and 33% of that in Case 1.

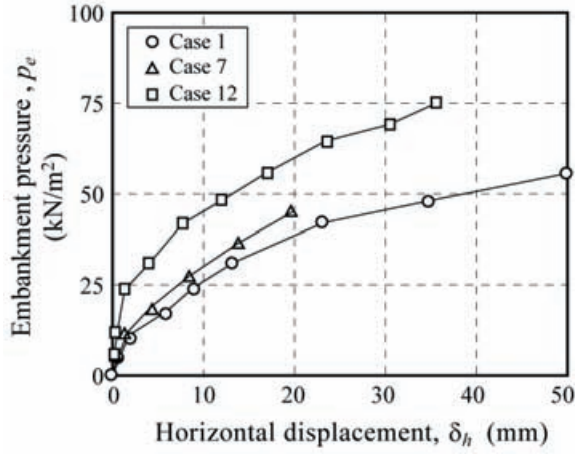

Fig. 3. Embankment pressure and horizontal displacement curves.

In order to investigate the effect of column failure in detail, the $\delta_h - p_e$ curves of Cases 12 and 7 are plotted again in Figs. 4(a) and 4(b). In the figure, the letters beside the curves indicate the point in time and the ID number of the column that shows rupture breaking failure (Kitazume and Maruyama, 2007). The column ID is numbered as Row 1, 2, 3 and so on from the forefront column, and Line a, b, c and so on from the window, as shown in Fig. 2.

In Case 12 (Fig. 4(a)), one of the forefront columns, Tl-1d, failed first at p_e of 30.3 kN/m^2. As p_e increased, the other forefront column, Tl-1c, failed. Several second- and fourth-row columns failed one by one at p_e of 40.8 kN/m^2. At further loading steps, the forefront and third to fifth rows of columns failed one by one.

In Case 7 (Fig. 4(b)), one of the forefront columns, Tl-1b, failed first at p_e of 26.2 kN/m^2, and the second- and third-row columns, Tl-2b, Tl-2d and Tl-3c, failed at the same time. As p_e increased, the columns failed one by one in sequence from the forefront to the rearmost column.

Comparing these test cases, the embankment pressure, p_e, at the first column failure was about 15% larger in Case 12 than in Case 7, and the sequence of column failure was slightly different: the columns failed roughly in sequence from the forefront to the rearmost column in Case 7 but failed randomly in Case 12.

Based on the above results, the DM columns did not fail simultaneously but failed one by one in bending failure mode.

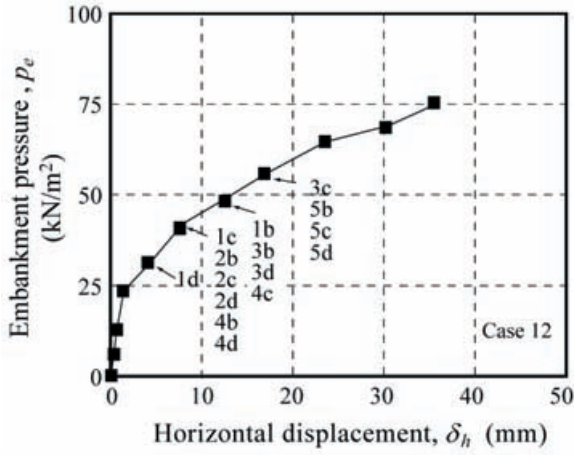

(a) Case 12

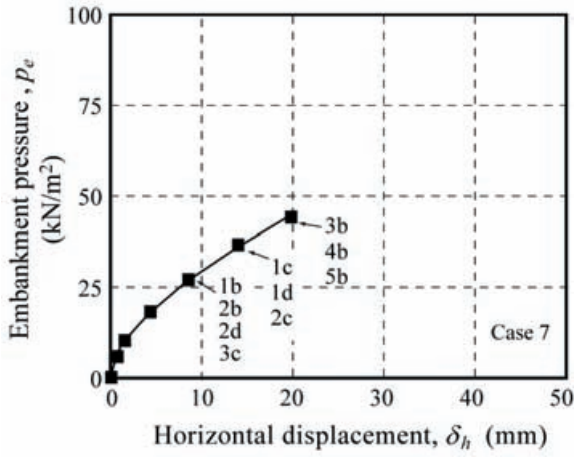

(b) Case 7

Fig. 4. Embankment pressure and horizontal displacement curves together with column failure.

It is of interest to note that the embankment pressure continued to increase even after the failure of many columns, irrespective of the surface improvement layer.

3.2 Embankment pressure at ground failure and improvement width

As shown in Fig. 4, neither a clear peak nor constant value can be seen in the $\delta_h - p_e$ curves even after the failure of many columns. Regarding the model test condi-

tions, the forefront column always failed first, irrespective of the surface improvement layer. A similar phenomenon was found irrespective of the column strength and the number of column rows (Kitazume and Maruyama, 2007). Here, ground failure is defined as the rupture breaking failure of the forefront column. The embankment pressure at ground failure, p_{ef}, is summarized in Table 2, and the relationship to the improvement width, D, is plotted in Fig. 5 together with the other test cases. As discussed in Fig. 4, the model columns failed one by one at several embankment pressures even in the forefront column. The pressure ranges at which the forefront columns failed are plotted as arrows. It can be seen that p_{ef} increased with increasing improvement width, D, and p_{ef} in Case 12 was about 15 to 35% larger than that in Case 7.

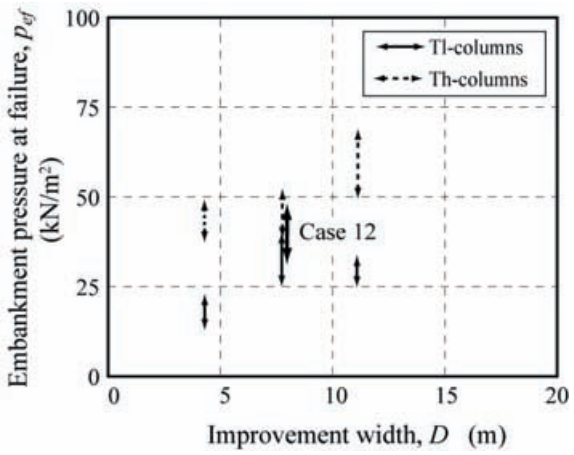

Fig. 5. Embankment pressure at ground failure and improvement width.

3.3 Column failure

The model ground was excavated after the embankment loading to observe the DM columns in detail. Figures 6(a) and 6(b) show the column failure in Cases 12 and 7, respectively.

In Case 12 (Fig. 6(a)), all the columns broke at several depths due to being subjected to considerably large embankment pressure. The figure clearly shows that the column did not fail by shear failure mode but by bending failure mode. Several tensile cracks developed in the forefront column, Tl-1d, and the column titled counterclockwise. In the second-row column, Tl-2d, several tensile cracks also developed. The electric measurement of the carbon rod did not show which crack developed first. However, according to the detailed observation after the test, bending failure can be assumed to have taken place at a shallow depth first and then at a deep depth. The detailed observation indicates that the tensile crack at the deeper depth developed from the right-hand side to the left and the column titled counterclockwise, but the tensile crack at the shallower depth developed from the left-hand side to the right and the column titled clockwise. This phenomenon can be clearly observed in the third to the fifth (the rearmost) columns. This indicates that the large clockwise moment load took place at a shallow depth due to the surface improvement layer.

In Case 7, as shown in Fig. 6(b), all the columns tilted counterclockwise with tensile cracks at two depths even when the embankment loading was terminated at a relatively low pressure. The figure clearly shows that the column did not fail by shear failure mode but by bending failure mode. According to Fig. 4(b), Tl-1b and Tl-2b failed first and then the other three columns, Tl-3b, Tl-4b and Tl-5b, failed at the same p_e of 43.9 kN/m^2. As discussed earlier, it is reasonable to assume that bending failure took place in these columns, one by one. According to the detailed observation after the test, bending failure took place at a shallow depth first and then at a deep depth. Counterclockwise displacement can be seen in Tl-1b and Tl-2b; however, the top of the rearmost column, Tl-5b, inclined slightly clockwise, due to large ground settlement beneath the embankment (Kitazume and Maruyama, 2007).

It is of interest to note that the location of the bending failure is deeper in the improved ground with the surface improvement layer (Case 12) compared to that without the surface improvement layer (Case 7).

(a) Case 12 (Line d)

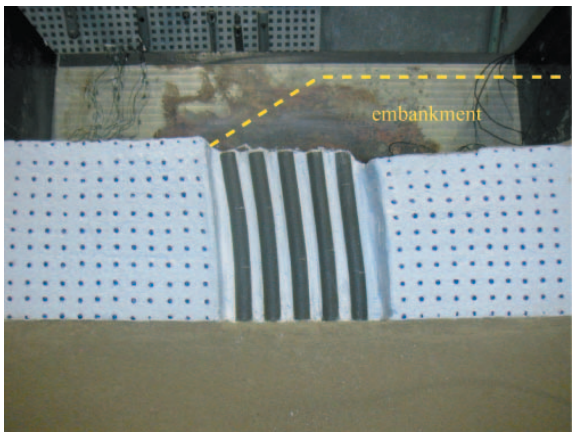

(b) Case 7 (Line b)

Fig. 6. Column failure.

3.4 Failure of surface improvement layer

In Case 12, two carbon rods were embedded parallel to the specimen length in the surface improvement layer to detect the failure, similar to the columns. Figure 7 shows a top view of the surface improvement layer after the embankment loading, with the embedded position of the carbon rods indicated by broken yellow lines. The measurements of the rods show that the surface layer was broken at the rear side first and then at the window side at an embankment pressure of 30.3 and 40.8 kN/m^2, respectively. A tensile crack developed just behind the rearmost column and extended over the entire length of the layer. However, no failure took place in other parts of the layer.

Fig. 7. Surface improvement layer failure.

3.5 Ground deformation

The ground deformation is shown in Fig. 8 for the improved ground with and without the surface improvement layer (Cases 12 and 7). The data was obtained by digitizing the coordinates of the target markers placed on the side surface of the model ground, which corresponds to the ground deformation of the clay between the columns. In Case 12 (Fig. 8(a)), relatively large ground deformation can be seen at shallow and intermediate depths. The clay ground was displaced almost horizontally in the improved portion, but moved downward at the rear and upward at the front. The ground deformation in Case 7 (Fig. 8(b)) is very similar to that in Case 12, irrespective of the surface improvement layer, where no slip circle failure was observed.

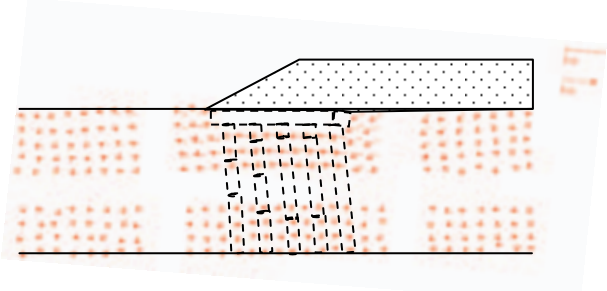

(a) Case 12 at embankment pressure of 47.6 kN/m^2

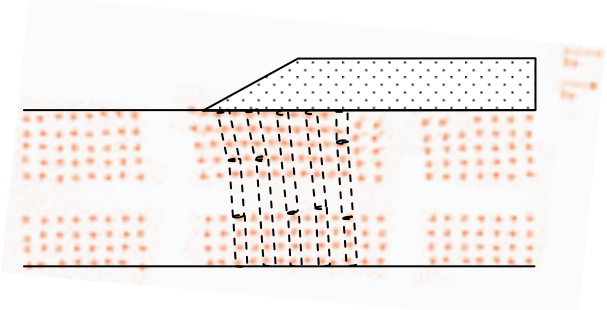

(b) Case 7 at embankment pressure of 43.9 kN/m^2

Fig. 8. Ground deformation.

3.6 Horizontal displacement distribution

In order to investigate the ground deformation in detail, the horizontal displacement distribution with depth measured at the toe of the embankment slope is shown in Fig. 9 for the improved ground with and without the surface improvement layer (Cases 12 and 7), in which the horizontal displacement measured at various loading stages is plotted.

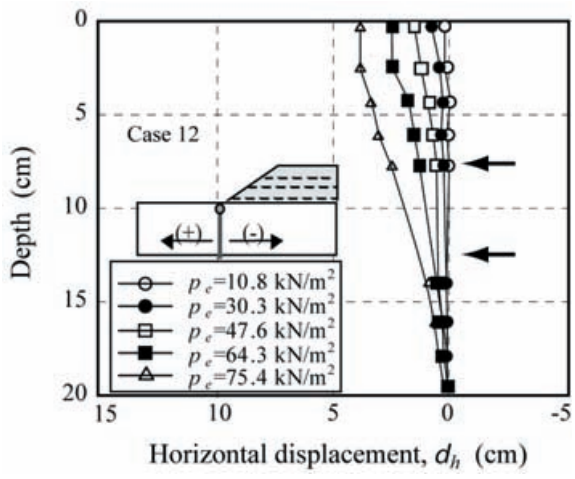

(a) Improved ground (Case 12)

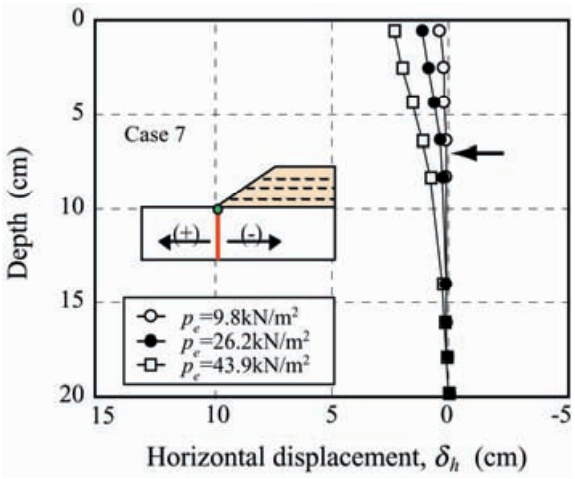

(b) Improved ground (Case 7)

Fig. 9. Horizontal displacement distribution with depth.

In Case 12 (Fig. 9(a)), horizontal displacement at the toe of the embankment slope, corresponding to the forefront column, developed with increasing p_e, but its distribution was almost linear with the depth throughout the embankment loading. The horizontal displacement at the bottom of the column is negligible. As the front surface of the ground on which the target markers were placed corresponds to the intermediate point between the columns, the clay between the columns did not squeeze through but instead was displaced together with the columns. These observations indicate that the improved area did not fail. In the figure, the locations of the forefront column failure are plotted as arrows. The horizontal displacement distribution was almost a linear shape even after the columns failed.

In Case 7, Fig. 9(b), a similar phenomenon can be seen, where horizontal displacement developed with increasing p_e, but its distribution was almost linear with the depth throughout the embankment loading. In the figure, the location of the forefront column failure is also plotted as

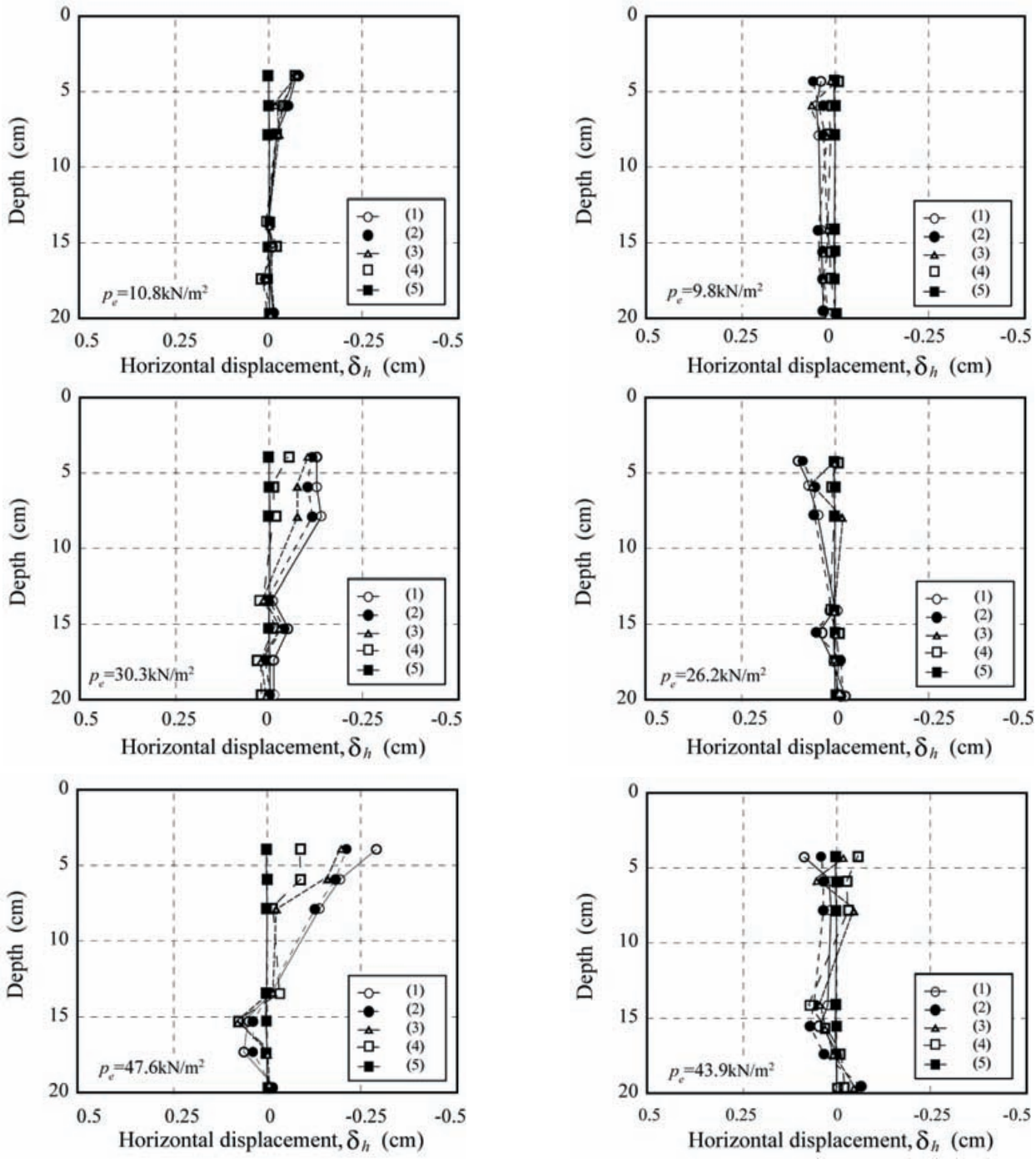

(a) Improved ground (Case 12) (b) Improved ground (Case 7)

Fig. 10. Horizontal displacement distribution with depth.

an arrow. The horizontal displacement distribution was also almost a linear shape even after the columns failed.

Comparing the two cases, the horizontal displacement in Case 12 is smaller than that in Case 7, which indicates that the surface improvement layer had a large effect on reducing the horizontal displacement.

In order to investigate the horizontal displacement in detail, the distribution in Fig. 9 is re-plotted in Fig. 10, where the increments in horizontal displacement with respect to the rearmost column are plotted.

The numbers in the figure, (1), (2) to (5), indicate the horizontal position of the clay ground corresponding to the foremost column, the second column, to the rearmost column, respectively (see Fig. 2). In Case 12 (Fig. 10(a)), the displacement at all columns shows a negative value and the magnitude becomes a larger negative value with increasing embankment pressure. This indicates that the clay ground between the foremost and rearmost columns was subjected to horizontal compressive deformation due to the embankment loading.

In Case 7 (Fig. 10(b)), however, without the surface improvement layer, the increment in horizontal displacement at every column was quite small, although there was scattering in the measured data. This indicates that the clay ground between the foremost and rearmost columns moved horizontally with negligible compressive deformation.

3.7 Vertical displacement distribution

The vertical displacement distribution of the clay ground with width measured at the ground surface is shown in Fig. 11 for the improved ground with and without the surface improvement layer, in which the vertical displacement measured at various loading stages is plotted.

In Case 12 (Fig. 11(a)), the improved ground with the surface improvement layer, the vertical displacement of the clay ground remained quite small in magnitude as long as the embankment pressure was low. However, when the embankment pressure exceeded about 64.3 kN/m^2, considerable settlement took place in the ground at the rear side of the surface improvement layer while large heaving occurred at the front side. This phenomenon clearly shows that the displacement of the surface improvement layer was a clockwise rotational movement.

In Case 7 (Fig. 11 (b)), almost uniform vertical settlement took place along the surface layer with increasing embankment pressure.

3.8 Vertical stress at top of columns

Figures 12(a) and 12(b) show the vertical stress increment during the embankment loading, which was measured at the top surface of the surface improvement layer in Case 12.

For vertical stress on the column as shown in Fig. 12(a), the vertical stress on the rearmost column increased very rapidly to a peak value at p_e of about 40 kN/m^2. The vertical stress on the other columns increased gradually, and some columns showed no peak value but instead remained almost constant. The stress increment was highest at the rearmost column and declined toward the foremost column, which corresponded to the triangle shape

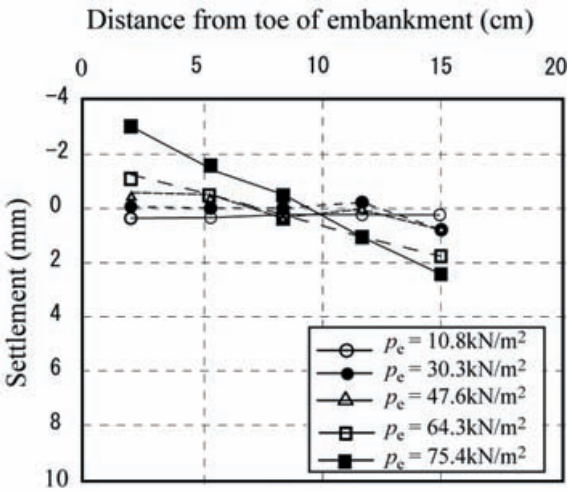

(a) Improved ground (Case 12)

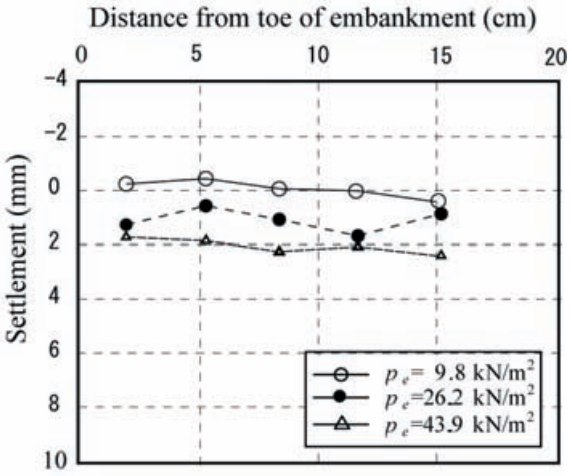

(b) Improved ground (Case 7)

Fig. 11. Vertical displacement distribution.

of the embankment on the surface improvement layer. In the figure, the arrows beside the curves indicate the point in time of the column failure. The time of the peak stress did not coincide with the time of column failure, but instead the columns failed after the vertical stress peaked.

For the vertical stress on the clay portion as shown in Fig. 12(b), the vertical stress between the rearmost and the second rearmost columns increased monotonically with increasing p_e. Its magnitude was almost of the same order as p_e, which was almost of the same order as the vertical stress on the rearmost column (Fig. 12(a)). The vertical stress at the other positions also increased rapidly at first and then reached almost a constant value.

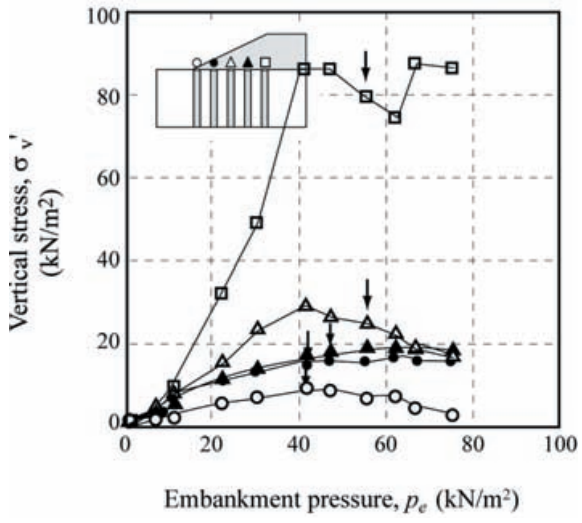

(a) On the column

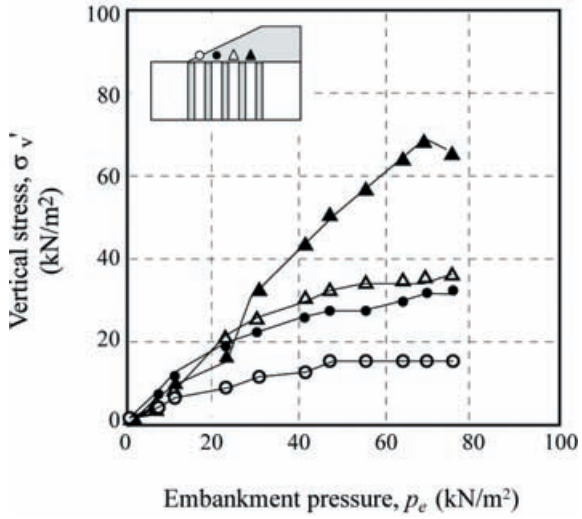

(b) On the clay

Fig. 12. Vertical stress and embankment pressure curves.

3.9 Stress concentration ratio

Figures 13(a) and 13(b) show the stress concentration ratio, n, in Cases 12 and 7, which is defined by the ratio of the vertical stress increment at the top of the column against that at the clay surface between the columns.

In Case 12 (Fig. 13(a)), the n value at Tl-5c increased with increasing p_e to a peak value at p_e of about 25 kN/m^2. After peaking, the n value decreased once and then increased again to show another peak at p_e of about 40 kN/m^2. Finally, the n value decreased to almost unity with further increasing of p_e. The others are lower than unity. This phenomenon is quite different from that in Case 7 (Fig. 13(b)). It can be concluded that the embankment pressure was not concentrated in the DM columns in the improved ground with the surface improvement layer, due to the high stiffness of the surface layer.

In Case 7 (Fig. 13(b)), the n value temporarily decreased at the first loading step but increased with increasing p_e and reached a peak in columns Tl-2c and Tl-3c. The n value at Tl-1c to Tl-3c was quite low, lower than unity, because the stress increment at the top of the column was quite low (Kitazume and Maruyama, 2007). In columns Tl-4c and Tl-5c, the n value continued to increase with increasing p_e and had no peak. Although the n value varied for each column and embankment loading level, a high value was obtained at the rear side columns.

The n value is usually obtained by direct measurement of the stress, or by back calculation of ground settlement in the field. Accumulated data shows the n value ranging from 10 to 20 (CDIT, 2002), which is considerably higher than in this study. It can be concluded that the surface improvement layer had the effect of reducing the stress concentration phenomenon.

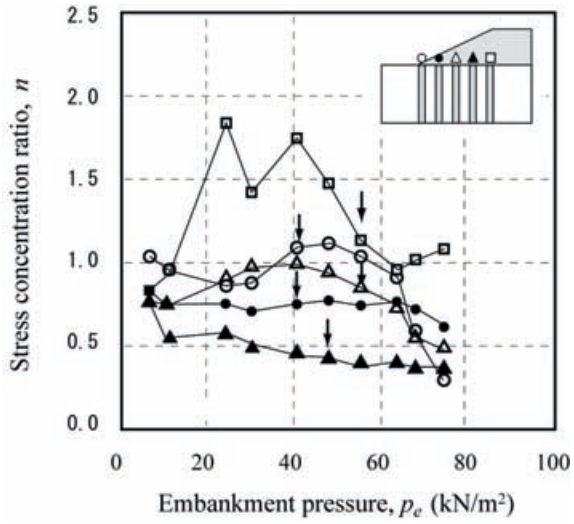

(a) Case 12

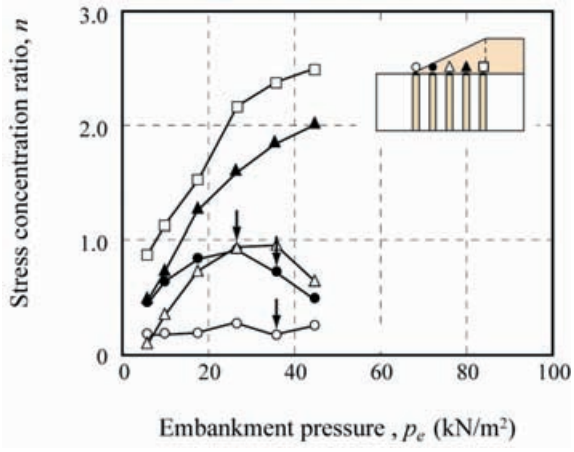

(b) Case 7

Fig. 13. Stress concentration ratio and embankment pressure curves.

4. DISCUSSION

The following discussion evaluates the effect of the surface improvement layer on a prototype scale instead of the model scale.

The evaluation of improved ground without a surface improvement layer was discussed in previous research (Kitazume and Maruyama, 2007, 2008), which revealed that the current design method based on the shear failure mode cannot reasonably evaluate the embankment pressure at failure and the depth of the failure plane, but a simple calculation based on the bending failure mode of the columns has relatively high applicability for evaluating the internal stability of the group column type improved ground. Here, the effect of the surface improvement layer is discussed based on the bending failure mode of the columns.

The improved group composed of the columns and the surface improvement layer can be considered as a sort of Rahmen structure. Ideally, its stability and behavior should be evaluated according to the Rahmen concept. However, as the interaction between the improved ground and the surrounding soft soil is too complex to obtain sufficient and precise information for the evaluation, it would be reasonable to evaluate the stability using a simplified method for practical purposes.

In the case of the improved ground with the surface improvement layer, two potential failures of DM columns should be evaluated as schematically shown in Fig. 14: (a) bending failure at a deep depth and (b) bending failure at a shallow depth. In the former case, the DM columns are assumed to fail by counterclockwise moment. In the later case, the DM columns are assumed to fail by induced moment due to the restriction by the surface improvement layer. Here, the criteria for each failure pattern are discussed individually first and then the combined failure criteria are discussed.

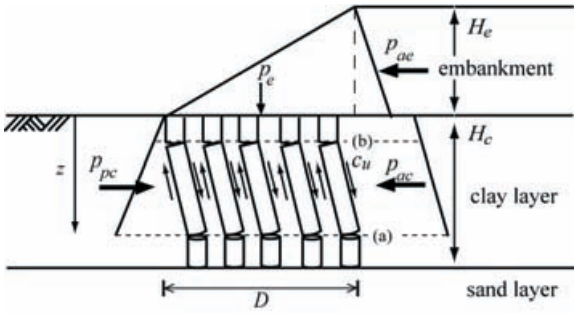

Fig. 14. Bending failure mode.

4.1 Column failure at deep depth (a)

Here, the simple stability calculation proposed in the previous research is modified to incorporate the effect of the surface improvement layer. Similar to the previous research, all the DM columns are assumed to simultaneously fail in bending failure mode. However, the assumption of full mobilization of bending strength does not correspond to the model test results where the columns fail one by one. In the calculation, the column is assumed to fail when the induced tensile stress reaches the ultimate bending strength, $\sigma_b = \alpha\, q_u$, where the α value is assumed as 0.28 (Kitazume and Maruyama, 2007). For the calculation, the moment equilibrium at the assumed failure plane, z, is analyzed as follows.

As discussed in Fig. 14, the clockwise moment is induced in the column at the surface improvement layer. Its magnitude, M_{sl}, can be calculated as Eq. (1) with the boundary condition of no rotational displacement at the top.

$$M_{sl} = \left(\gamma_e \cdot H_e \cdot \frac{L^2}{6} - \frac{2}{3} \cdot c_{u0} \cdot L^2 - \frac{1}{6} \cdot k \cdot L^3 \right) - \frac{B^2}{S} \cdot \left(\frac{1}{2} \cdot c_{u0} \cdot L + \frac{1}{6} \cdot k \cdot L^2 \right) \quad (1)$$

where

- B : Diameter of DM column (m)
- c_{u0} : Undrained shear strength of clay ground at the ground surface (kN/m^2)
- H_e : Height of embankment (m)
- k : Increment ratio of undrained shear strength of clay with depth (kN/m^3)
- L : Length of DM column (m)
- M_{sl} : Bending moment induced at the top of the DM column (kN×m)
- S : Spacing of DM columns (m)
- γ_e : Unit weight of embankment (kN/m^3)

The driving moments by the active earth pressure of the embankment, M_{ae}, and of the clay ground, M_{ac}, per unit breadth are expressed as Eqs. (2) and (3), respectively, where Rankine's theory on earth pressure is employed:

$$M_{ae} = \gamma_e \cdot H_e \cdot \tan^2\left(\frac{\pi}{4} - \frac{\phi_e}{2}\right) \cdot \frac{{H_e}^2 + 3 \cdot H_e \cdot z}{6} \quad (2)$$

$$M_{ac} = \frac{z^2}{6} \cdot \left(3 \cdot \gamma_e \cdot H_e + \gamma_c \cdot z - 6 \cdot c_{u0} - 2 \cdot k \cdot z\right) \quad (3)$$

The resistance moments per unit breadth by the adhesion mobilizing on the side surface of DM columns, M_{rc}, by the weight of DM columns, M_{rt}, by the weight of embankment on DM columns, M_{re}, by the shear strength of clay between DM columns, M_{sc}, by the passive earth pressure of clay ground, M_{pc}, and by the bending failure of DM columns, M_{pb}, are expressed as Eqs. (4) through (9), respectively.

$$M_{rc} = B^2 \cdot z \cdot \frac{2 \cdot c_{u0} + k \cdot z}{2} \cdot N \cdot \frac{1}{S} \quad (4)$$

$$M_{rt} = \frac{\pi}{8} B^3 \cdot z \cdot \gamma_t \cdot N \cdot \frac{1}{S} \quad (5)$$

$$M_{re} = \frac{\pi}{8} B^3 \cdot H_e \cdot \gamma_e \cdot \frac{n}{1+(n-1)\cdot a_s} \cdot N \cdot \frac{1}{S} = \frac{\pi}{8} B^3 \cdot H_e \cdot \gamma_e \cdot \mu_s \cdot N \cdot \frac{1}{S} \quad (6)$$

$$M_{sc} = S \cdot (1-a_s) \cdot \frac{2 \cdot c_{u0} + k \cdot z}{2} \cdot (N-1) \cdot z \quad (7)$$

$$M_{pc} = \frac{z^2}{6} \cdot (\gamma_c \cdot z + 4 \cdot c_{u0} + 2 \cdot k \cdot z) \quad (8)$$

$$M_{pb} = \frac{\pi}{32} \cdot B^3 \cdot \sigma_b \cdot N \cdot \frac{1}{S} = \frac{\pi}{32} \cdot B^3 \cdot \alpha \cdot q_u \cdot N \cdot \frac{1}{S} \quad (9)$$

where

- M_{ac} : Driving moment by active earth pressure of clay ground (kN×m)
- M_{ae} : Driving moment by active earth pressure of embankment (kN×m)
- M_{rc} : Resistance moment by adhesion on side surface of DM columns (kN×m)
- M_{re} : Resistance moment by weight of embankment (kN×m)
- M_{rt} : Resistance moment by weight of DM columns (kN×m)
- M_{sc} : Resistance moment by shear strength of clay between DM columns (kN×m)
- M_{pc} : Resistance moment by passive earth pressure of clay ground (kN×m)
- M_{pb} : Bending moment of DM column (kN×m)
- n : Stress concentration ratio
- N : Number of DM column rows
- α : Bending strength ratio to unconfined compressive strength
- γ_c : Unit weight of clay ground (kN/m^3)
- γ_t : Unit weight of DM column (kN/m^3)
- ϕ_e : Internal friction angle of embankment (°)
- μ_s : Stress concentration coefficient
- σ_b : Bending strength (kN/m^2)

According to the moment equilibrium at the failure plane, the following equation should be satisfied:

$$M_{ae} + M_{ac} = M_{rc} + M_{rt} + M_{re} + M_{sc} + M_{pc} + M_{pb} + M_{sl} \quad (10)$$

After substituting Eqs. (1) through (9) into Eq. (10) and expanding the equation, the following cubic equation is obtained with respect to the embankment height, H_e:

$$\begin{aligned} &-\frac{\gamma_e}{6} \cdot \tan\left(\frac{\pi}{4} - \frac{\phi_e}{2}\right) \cdot H_e^3 - \frac{\gamma_e}{2} \cdot \tan\left(\frac{\pi}{4} - \frac{\phi_e}{2}\right) \cdot z \cdot H_e^2 \\ &+ \{D \cdot \left(\frac{4}{\pi} \cdot a_s \cdot \frac{2 \cdot c_{u0} + k \cdot z}{2} + \frac{1}{2} \cdot a_s \cdot B \cdot \gamma_e \cdot \mu_s \cdot \frac{1}{S}\right. \\ &\left. - (1-a_s) \cdot \frac{2 \cdot c_{u0} + k \cdot z}{2}\right) - \frac{z^2}{2} \cdot \gamma_e \cdot \frac{1}{S}\} \cdot H_e \\ &+ \{a_s \cdot B \cdot z \cdot \gamma_t \cdot \frac{1}{S} + \frac{z^2}{3} \cdot (6 \cdot c_{u0} + 2 \cdot k \cdot z) \\ &+ \frac{\pi}{32} \cdot B^3 \cdot \alpha \cdot q_u \cdot N \cdot \frac{1}{S} - \left(\gamma_e \cdot H_e \cdot \frac{L^2}{6} - \frac{2}{3} \cdot c_{u0} \cdot L^2 - \frac{1}{6} \cdot k \cdot L^3\right) \\ &+ \frac{B^2}{S} \cdot \left(\frac{1}{2} \cdot c_{u0} \cdot L + \frac{1}{6} \cdot k \cdot L^2\right)\} = 0 \end{aligned}$$

Three solutions, either three real numbers or one real and two imaginary numbers, are obtained by Cardano's formula. A meaningful solution for this study would be a real number and positive value. As there are many variables in the equation, a solution, $H_{ef,bending}$, is numerically calculated for specific ground conditions and assumed bending failure plane, z. The embankment pressure at ground failure, $p_{ef,bending}$, is calculated by Eq. (12):

$$p_{ef,binding} = \gamma_e \cdot H_{ef,bending} \quad (12)$$

Figure 15 shows the relationship between the assumed depth of the failure plane, z, and p_e for the improved ground with D = 7.7 m and a_s = 0.28. The relationship for various column strengths is plotted in the figure and shows a concave shape, irrespective of the q_u value. The $z_{f,bending}$ giving $p_{ef,bending}$, as shown by the arrow, increases slightly with increasing q_u. The relationship is a relatively flat concave shape irrespective of the column strength, which means that the $z_{f,bending}$ can easily be variable due to a slight change in ground conditions. It can be seen that $p_{ef,bending}$ also increases slightly with increasing q_u.

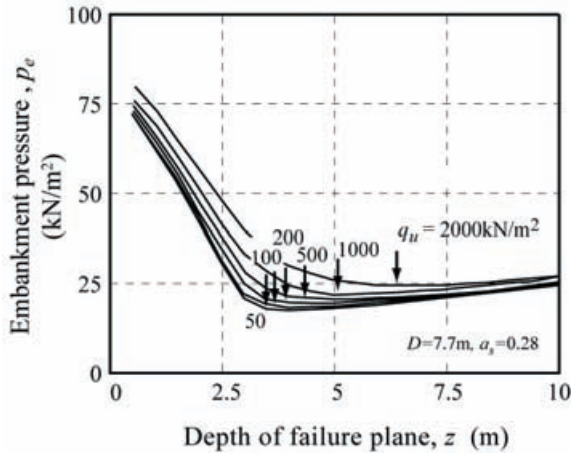

Fig. 15. Assumed depth of failure plane and embankment pressure for Case 12.

A series of calculations was carried out for various improvement widths and column strengths, and the relationship between D and $z_{f,bending}$ is shown in Fig. 16(a) for the improved ground with the surface improvement layer. The $z_{f,bending}$ value increases monotonically with increasing D and with increasing q_u. It is of interest to note that the $z_{f,bending}$ value is comparatively small for q_u of 50 kN/m^2 but becomes much larger when q_u is 100 kN/m^2 or higher. Figure 16(b) shows an example for the improved ground without the surface improvement layer for comparison (Kitazume and Maruyama, 2007). The effect of D and q_u on $z_{f,bending}$ for the improved ground with the surface improvement layer is much more dominant than without the surface layer.

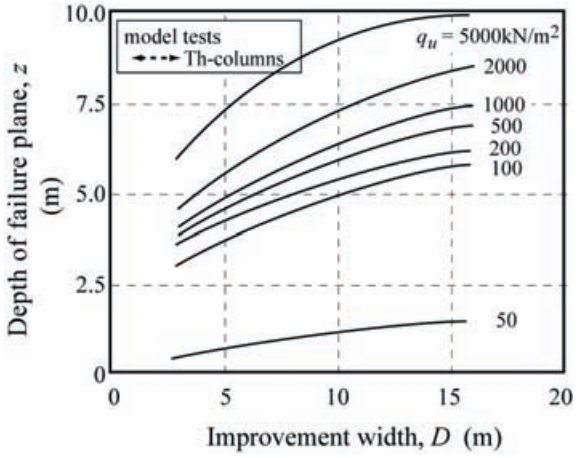

(a) Improved ground with surface improvement layer

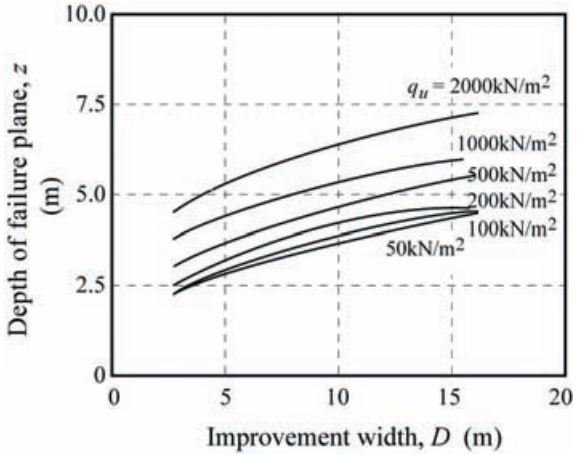

(b) Improved ground without surface improvement layer

Fig. 16. Failure depth and improved width of failure plane (a).

The $p_{ef,bending}$ value is shown along with D in Fig. 17 for the improved ground with and without the surface improvement layer. As shown in Fig. 17(a), the $p_{ef,bending}$ value increases monotonically with increasing D and q_u for the ground with the surface improvement layer. A similar phenomenon can also be seen for the ground without the surface improvement layer, as shown in Fig. 17(b). The improvement width, D, has a dominant effect on $p_{ef,bending}$, but the column strength, q_u, does not, irrespective of the surface improvement layer.

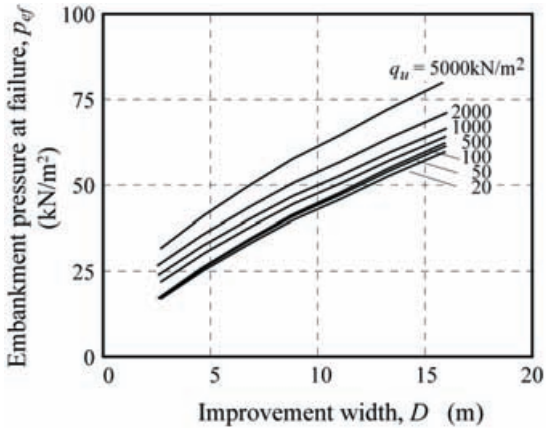

(a) Improved ground with surface improvement layer

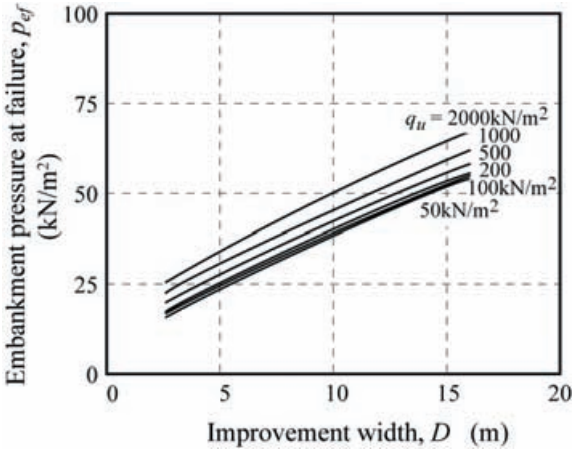

(b) Improved ground without surface improvement layer

Fig. 17. Embankment pressure at ground failure and improvement width of failure plane (a).

4.2 Column failure at shallow depth (b)

As discussed in Fig. 14, the clockwise moment is induced at the top of the column due to the effect of the surface improvement layer. Its magnitude, M_{sl}, formulated as Eq. (1), increases linearly with increasing embankment pressure. In the calculation, the column is assumed to fail when the induced tensile stress due to M_{sl} reaches the ultimate bending strength, σ_b, of the DM column. The embankment pressure at the column top failure, p_{ef}, is calculated and plotted in Fig. 18. The figure shows that p_{ef} increases with increasing improvement width, D, and the column strength, q_u. In a comparison with Fig. 17(a), the effect of q_u on p_{ef} is much more dominant in Fig. 18. As the induced moment, M_{sl}, is not influenced by the column strength, q_u, the embankment pressure at failure for the column top failure increases considerably with increasing q_u.

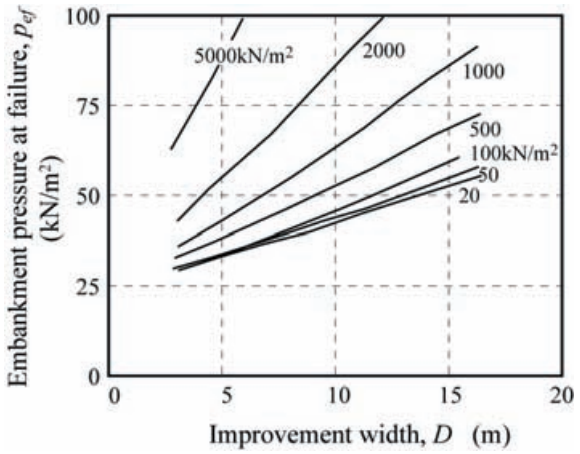

Fig. 18. Embankment pressure at ground failure and improvement width of failure plane (b).

4.3 Combined failure criteria for DM column

It is reasonable that the DM column would fail by either of the two failure patterns that give the minimum capacity under certain conditions. Figure 19 shows the combination of failure criteria (a) and (b). It was found that p_{ef} increases with increasing D and q_u, and p_{ef} for the two failure criteria is almost of the same order as in the case where q_u is lower than about 500 kN/m^2. As the column strength of the test case was about 400 kN/m^2, as shown in Table 1, it can be estimated that two failures took place in the columns at almost the same time at deep and shallow depths. The criterion for failure plane (a) gives a lower p_{ef} value in almost all the cases in this study.

In the figure, the model test results are also plotted as arrows. The test results are plotted within the calculation for various p_{ef} values, showing a reasonable estimation.

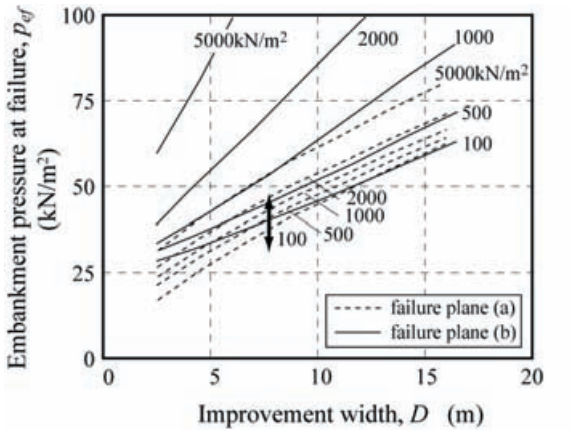

Fig. 19. Embankment pressure at ground failure and improvement width for combined planes.

4.4 Effect of surface improvement layer (embankment pressure at failure)

Table 3 shows the effect of surface layer on the embankment pressure at failure, p_{ef}. The p_{ef} value increases with the improvement width, D, and the column strength, q_u. The increase in p_{ef} due to the surface improvement layer is quite small, in the order of around 5%.

Table 3. Comparison of embankment pressure at failure.

Ground conditions		Embankment pressure at failure (kN/m^2)		
Column strength, q_u (kN/m^2)		D = 4.3 m	D = 7.6 m	D = 10.9 m
100	With surface layer	0.251	0.350	0.621
	Without surface layer	0.236	0.346	0.585
1000	With surface layer	0.296	0.421	0.676
	Without surface layer	0.287	0.400	0.644
2000	With surface layer	0.331	0.462	0.719
	Without surface layer	0.321	0.439	0.690

In order to investigate the effect of the surface improvement layer, the resistance moment components for failure plane (a) are shown in Fig. 20. The passive earth pressure component of the resistance moment, M_{pc}, increases with increasing q_u due to increasing $z_{f,bending}$. The passive earth pressure component, M_{pc}, has a dominant role in the entire resistance load throughout D. Its degree increases with decreasing D and with increasing q_u. The component of the clay strength between the columns, M_{sc}, also has a dominant role. However, the surface improvement layer component, M_{sl}, has quite a small role of about 5% of the entire resistance.

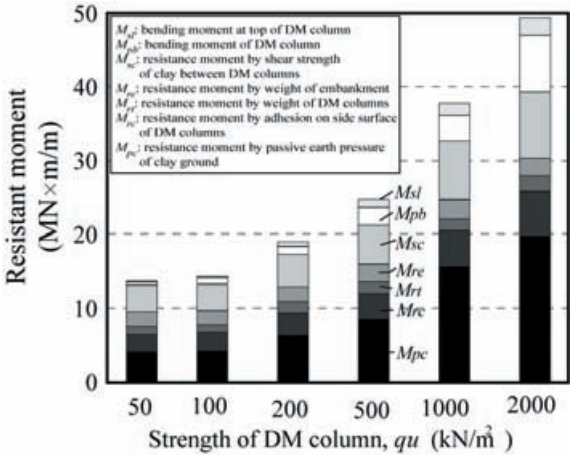

Fig. 20. Resistance moment components.

4.5 Effect of surface improvement layer (failure point)

A series of calculations was carried out for different improvement widths and column strengths, and the relationship between D and $z_{f,bending}$ is shown in Fig. 21 for various q_u values. The z_f value increases monotonically with increasing D, and with increasing q_u. In the figure, the model test results are also plotted. The calculation gives a reasonable estimation of the depth of the failure plane, slightly underestimated compared to the model test for Case 12.

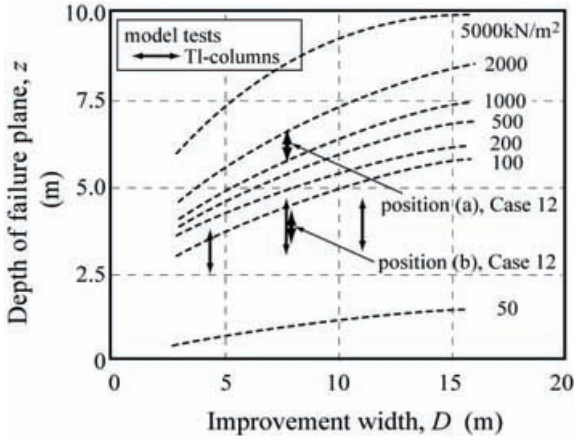

Fig. 21. Depth of failure plane (a) and improvement width.

5. CONCLUSIONS

The effect of the surface improvement layer on the failure pattern of group column type DM improved ground subjected to embankment loading was discussed through a series of centrifuge model tests and a simple calculation. As the number of test case with the surface improved layer was one, further tests with various conditions should be carried out to investigate the effect of the surface layer more precisely. The major conclusions derived in this study are as follows:

1) The embankment pressure increases monotonically with increasing ground displacement without a peak, irrespective of the surface improvement layer even after many DM columns fail.
2) The embankment pressure at ground failure is about 15 to 35% larger in the improved ground with the surface improvement layer compared to that without the surface improvement layer.
3) The DM columns do not fail simultaneously but instead fail one by one. The failure location of the DM columns is deeper in the improved ground with the surface improvement layer compared to that without the surface improvement layer.
4) The surface improvement layer has the effect of reducing the horizontal displacement and the stress concentration phenomenon.
5) The simple calculation based on the bending failure mode of the columns has relatively high applicability for evaluating the internal stability of the group column type improved ground with the surface improvement layer.
6) The importance of simulating a suitable failure pattern of improved ground is demonstrated for accurately evaluating the internal stability.

(*Received on November 8, 2010*)

NOTATION

B : Diameter of DM column (m)
c_{u0} : Undrained shear strength of clay ground at the ground surface (kN/m^2)
H_e : Height of embankment (m)
k : Increment ratio of undrained shear strength of clay with depth (kN/m^3)
L : Length of DM column (m)
M_{ac} : Driving moment by active earth pressure of clay ground (kN×m)
M_{ae} : Driving moment by active earth pressure of embankment (kN×m)
M_{pb} : Bending moment of DM column (kN×m)
M_{pc} : Resistance moment by passive earth pressure of clay ground (kN×m)
M_{rc} : Resistance moment by adhesion on side surface of DM columns (kN×m)
M_{re} : Resistance moment by weight of embankment (kN×m)
M_{rt} : Resistance moment by weight of DM columns (kN×m)
M_{sc} : Resistance moment by shear strength of clay between DM columns (kN×m)
M_{sl} : Bending moment induced at the top of the DM column (kN×m)
n : Stress concentration ratio
N : Number of DM column rows
q_u : Unconfined compressive strength (kN/m^2)
S : Spacing of DM columns (m)
α : Bending strength ratio to unconfined compressive strength
γ_c : Unit weight of clay ground (kN/m^3)
γ_e : Unit weight of embankment (kN/m^3)
γ_t : Unit weight of DM column (kN/m^3)
ϕ_e : Internal friction angle of embankment (°)
μ_s : Stress concentration coefficient
σ_b : Bending strength (kN/m^2)

REFERENCES

1) Broms, B.B. (2004): "Lime and lime/cement columns," Ground Improvement, 2nd edition, edited by M.P. Moseley and K. Kirsch, Spon Press, pp. 252-330.
2) Coastal Development Institute of Technology (2002): "The

Deep Mixing Method – Principle, Design and Construction," A.A. Balkema Publishers, 123p.

3) Hashizume, H., Okochi, Y., Dong, J., Horii, N., Toyosawa, Y. and Tamate, S. (1998): "Study on the behavior of soft ground improved using deep mixing method," Proc. of the International Conference Centrifuge 98, pp. 851-856.

4) Japan Society of Civil Engineers (2002): Standard Specifications for Concrete Structures – 2002, Method of testing for flexural strength of concrete (JIS A 1106-1999), pp. 291-294 (in Japanese).

5) Karastanev, D., Kitazume, M., Miyajima, S. and Ikeda, T. (1997): "Bearing capacity of shallow foundation on column type DMM improved ground," Proc. of the 14th International Conference on Soil Mechanics and Foundation Engineering, Vol. 3, pp. 1621-1624.

6) Kitazume, M. (2008): "Stability of Group Column Type DM Improved Ground under Embankment Loading," Report of the Port and Airport Research Institute, Vol. 47, No. 1, pp. 1-53.

7) Kitazume, M., Ikeda, T., Miyajima, S. and Karastanev, D. (1996): "Bearing capacity of improved ground with column type DMM," Proc. of the 2nd International Conference on Ground Improvement Geosystems, Vol. 1, pp. 503-508.

8) Kitazume, M. and Maruyama, K. (2005): "Collapse failure of group column type deep mixing improved ground under embankment," Proc. of the International Conference on Deep Mixing – Best Practice and Recent Advances, Vol. 1.2, pp. 245-254.

9) Kitazume, M. and Maruyama, K. (2006): "External stability of group column type deep mixing improved ground under embankment," Soils and Foundations, Vol. 46, No. 3, pp. 323-340.

10) Kitazume, M. and Maruyama, K. (2007): "Internal Stability of Group Column Type Deep Mixing Improved Ground under Embankment Loading," Soils and Foundations, Vol. 47, No. 3, pp. 437-455.

11) Kitazume, M. and Miyajima, S. (1995): "Development of PHRI Mark II geotechnical centrifuge," Technical Note of the Port and Harbour Research Institute, No. 817, 33p.

12) Kitazume, M., Nakamura, T. and Terashi, M. (1991): "Reliability of clay ground improved by the group column type DMM with high replacement," Report of the Port and Harbour Research Institute, Vol. 30, No. 2, pp. 305-326 (in Japanese).

13) Kitazume, M., Yamamoto, M. and Udaka, Y. (1999): "Vertical bearing capacity of column type DMM ground with low improvement ratio," Proc. of the International Conference on Dry Mix Methods for Deep Soil Stabilization, pp. 245-250.

14) Kitazume, M., Okano, K. and Miyajima, S. (2000): "Centrifuge model tests on failure envelope of column type DMM improved ground," Soils and Foundations, Vol. 40, No. 4, pp. 43-55.

15) Kivelo, M. (1998): "Stabilization of embankments on soft soil with lime/cement columns," PhD Thesis, Royal Institute of Technology, Sweden, 170p.

16) Miyake, M., Akamoto, H. and Wada, M. (1991): "Deformation characteristics of ground improved by a group of treated soil," Proc. of the International Conference Centrifuge 1991, pp. 295-302.

17) Public Works Research Center (1999): "Design and Construction Manual on Deep Mixing Method for Inland Construction," 326p. (in Japanese).

18) Terashi, M., Tanaka, H., Mitsumoto, T., Niidome, Y. and Honma, S. (1980): "Fundamental properties of lime- and cement-treated soils (2nd Report)," Report of the Port and Harbour Research Institute, Vol. 19, No. 1, pp. 33-62 (in Japanese).

19) Terashi, M. and Tanaka, H. (1983): "Bearing capacity and consolidation of ground improved by a group of treated soil columns," Report of the Port and Harbour Research Institute, Vol. 22, No. 2, pp. 213-266 (in Japanese).

港湾空港技術研究所報告　第 50 巻第 1 号

２０１１．３

編集兼発行人　独立行政法人港湾空港技術研究所

発　行　所　独立行政法人港湾空港技術研究所
横須賀市長瀬３丁目１番１号
TEL. 046(844)5040　URL. http://www.pari.go.jp/

印　刷　所　株式会社シーケン

CONTENTS